

# Reassessing associations between white matter and behaviour with multimodal microstructural imaging

Alberto Lazari <sup>\*1</sup>, Piergiorgio Salvan<sup>1</sup>, Michiel Cottaar<sup>1</sup>, Daniel Papp<sup>1</sup>, Olof Jens van der Werf<sup>3,4</sup>, Ainslie Johnstone<sup>1, 5</sup>, Zeena-Britt Sanders<sup>1</sup>, Cassandra Sampaio-Baptista<sup>1</sup>, Nicole Eichert<sup>1</sup>, Kentaro Miyamoto<sup>6</sup>, Anderson Winkler<sup>7</sup>, Martina F. Callaghan<sup>8</sup>, Thomas E. Nichols<sup>9</sup>, Charlotte J Stagg<sup>1,2,10</sup>, Matthew Rushworth<sup>6</sup>, Lennart Verhagen<sup>6,11</sup>, and Heidi Johansen-Berg <sup>†1</sup>

<sup>1</sup> *Wellcome Centre for Integrative Neuroimaging, FMRIB, Nuffield Department of Clinical Neurosciences, University of Oxford*

<sup>2</sup> *Oxford Centre for Human Brain Activity, Wellcome Centre for Integrative Neuroimaging, Department of Psychiatry, University of Oxford*

<sup>3</sup> *Section Brain Stimulation and Cognition, Department of Cognitive Neuroscience, Faculty of Psychology and Neuroscience, Maastricht University, Maastricht, The Netherlands*

<sup>4</sup> *Maastricht Brain Imaging Centre (MBIC), Maastricht University, Maastricht, The Netherlands*

<sup>5</sup> *Department of Clinical and Movement Neuroscience, Institute of Neurology, University College London, WC1N 3BG*

<sup>6</sup> *Wellcome Centre for Integrative Neuroimaging, Department of Experimental Psychology, University of Oxford*

<sup>7</sup> *National Institute of Mental Health, National of Health, Bethesda, MD, USA*

<sup>8</sup> *Wellcome Centre for Human Neuroimaging, UCL Queen Square Institute of Neurology, UCL, London, UK*

<sup>9</sup> *Oxford Big Data Institute, Li Ka Shing Centre for Health Information and Discovery, Nuffield Department of Population Health, University of Oxford*

<sup>10</sup> *MRC Brain Network Dynamics Unit, University of Oxford, Oxford, OX1 3TH, UK*

<sup>11</sup> *Donders Institute for Brain, Cognition and Behaviour, Radboud University Nijmegen, Nijmegen, Netherlands*

---

<sup>\*</sup>alberto.lazari@univ.ox.ac.uk

<sup>†</sup>heidi.johansen-berg@ndcn.ox.ac.uk

## Abstract

Several studies have established specific relationships between White Matter (WM) and behaviour. However, these studies have typically focussed on fractional anisotropy (FA), a neuroimaging metric that is sensitive to multiple tissue properties, making it difficult to identify what biological aspects of WM may drive such relationships. Here, we carry out a pre-registered assessment of WM-behaviour relationships in 50 healthy individuals across multiple behavioural and anatomical domains, and complementing FA with myelin-sensitive quantitative MR modalities (MT, R1, R2\*).

Surprisingly, we only find support for predicted relationships between FA and behaviour in one of three pre-registered tests. For one behavioural domain, where we failed to detect an FA-behaviour correlation, we instead find evidence for a correlation between behaviour and R1. This hints that multimodal approaches are able to identify a wider range of WM-behaviour relationships than focusing on FA alone.

To test whether a common biological substrate such as myelin underlies WM-behaviour relationships, we then ran joint multimodal analyses, combining across all MRI parameters considered. No significant multimodal signatures were found and power analyses suggested that sample sizes of 40 to 200 may be required to detect such joint multimodal effects, depending on the task being considered.

These results demonstrate that FA-behaviour relationships from the literature can be replicated, but may not be easily generalisable across domains. Instead, multimodal microstructural imaging may be best placed to detect a wider range

of WM-behaviour relationships, as different MRI modalities provide distinct biological sensitivities. Our findings highlight a broad heterogeneity in WM's relationship with behaviour, suggesting that variable biological effects may be shaping their interaction.

## Highlights

- Pre-registered testing of microstructural imaging across modalities (FA, MT, R1, R2\*) to test WM-behaviour relationships.
- Partial support for FA-behaviour relationships hypothesised based on previous literature.
- Multimodal approaches can help detect WM-behaviour relationships that are not detected with FA alone.
- Sample sizes of 40 to 200 may be needed to detect myelin-behaviour relationships in joint multimodal analyses.
- Variable biological effects may be shaping WM-behaviour relationships.

## 1 **Introduction**

2 The past decade has shown that White Matter (WM), and in particular  
3 the myelinated structures that dominate it, have more varied functions than  
4 previously thought, from trophic support of axons (Fünfschilling et al., 2012;  
5 Nave, 2010) to active regulation of physiological and behavioural processes  
6 (Kaller et al., 2017; Lazari et al., 2018; Steadman et al., 2019). These  
7 basic biology findings suggest that WM may play a role in brain physiology  
8 and behaviour, and that WM could be targetted for therapeutic gain in  
9 neuropsychiatric disorders (Gibson et al., 2018; Vanes et al., 2020).

10 In humans, much evidence on the role of WM has come from a large body  
11 of studies linking behaviour to diffusion-tensor-based metrics such as fractional  
12 anisotropy (FA), a metric derived from diffusion weighted imaging that is sensitive  
13 to features of WM microstructure (Boekel et al., 2015; Johansen-Berg, 2010;  
14 Lazari and Lipp, 2020; Roberts et al., 2013). While these studies have provided  
15 seminal evidence for a link between WM and human behaviour, questions remain  
16 about the generalizability and interpretation of these effects.

17 FA-behaviour relationships are particularly difficult to interpret on a biological  
18 level. Diffusion signals are sensitive to a broad range of tissue properties,  
19 including myelination levels, fiber orientation, axon diameter, astrocyte and  
20 vascular morphology (Farquharson et al., 2013; Sampaio-Baptista and Johansen-  
21 Berg, 2017; Stolp et al., 2018). Therefore, a given FA-behaviour correlation could  
22 arise from a diversity of microstructural patterns (Zatorre et al., 2012). Moreover,  
23 while other tensor-based metrics can be derived from diffusion-weighted imaging,

24 it is unclear whether they differ from FA in their biological sensitivity (Lazari and  
25 Lipp, 2020).

26 In recent years, an increasing number of techniques (Figure 1) have been  
27 successfully applied to the study of WM, and of WM myelination in particular  
28 (Heath et al., 2018). As WM is dominated by myelinating oligodendrocytes,  
29 many of these techniques have focused on detecting direct signals from myelin or  
30 from iron, which is enriched in the cell body of oligodendrocytes. Magnetisation  
31 Transfer-based techniques, for example, quantify the fraction of macromolecule-  
32 bound water protons, and have been shown to relate strongly to myelination  
33 in a number of validation studies (Deloire-Grassin et al., 2000; Dousset et al.,  
34 1995, 1992). R2\* mapping, on the other hand, quantifies local field distortion  
35 caused by iron, and has been confirmed as an iron marker by several validation  
36 studies (Langkammer et al., 2010; Sun et al., 2015). R1 has gained attention  
37 recently as a quantitative metric for myelination, and although its effectiveness  
38 as a WM myelin marker has not been directly tested, it has been shown to detect  
39 spatial distributions of myelin in grey matter (Lutti et al., 2014; Stüber et al.,  
40 2014). In addition to the development of new MR techniques, new statistical  
41 tools, such as joint inference permutation testing (Winkler et al., 2014, 2016),  
42 facilitate the integration of Magnetic Resonance Imaging (MRI) techniques to  
43 clarify the biological interpretation of MRI-measured effects in white matter.

44 Applying these approaches to studying WM microstructural techniques could  
45 be helpful for clarifying the mechanisms behind WM-behaviour relationships. In  
46 particular, using MRI modalities that are sensitive to different biophysical tissue  
47 properties could disentangle whether myelination, oligodendrocytes, or fiber

48 orientation, or a combination of them, are key in driving reported FA-behaviour  
49 correlations. In turn, if all WM-behaviour relationships are driven by a common  
50 biological mechanism, then establishing recurrent multimodal patterns that  
51 correlate with behaviour could uncover it, with powerful implications for future  
52 studies looking at WM-behaviour relationships and biomarker development.

53 To tackle these open questions regarding WM-behaviour relationships, we set  
54 out to:

- 55 1) Perform confirmatory, pre-registered testing of FA-behaviour relationships.
- 56 2) Perform pre-registered testing of relationships between behaviour and  
57 microstructural imaging across neuroimaging modalities.
- 58 3) Identify multimodal microstructural signatures which may provide insights  
59 into the underlying biology of WM-behaviour relationships.

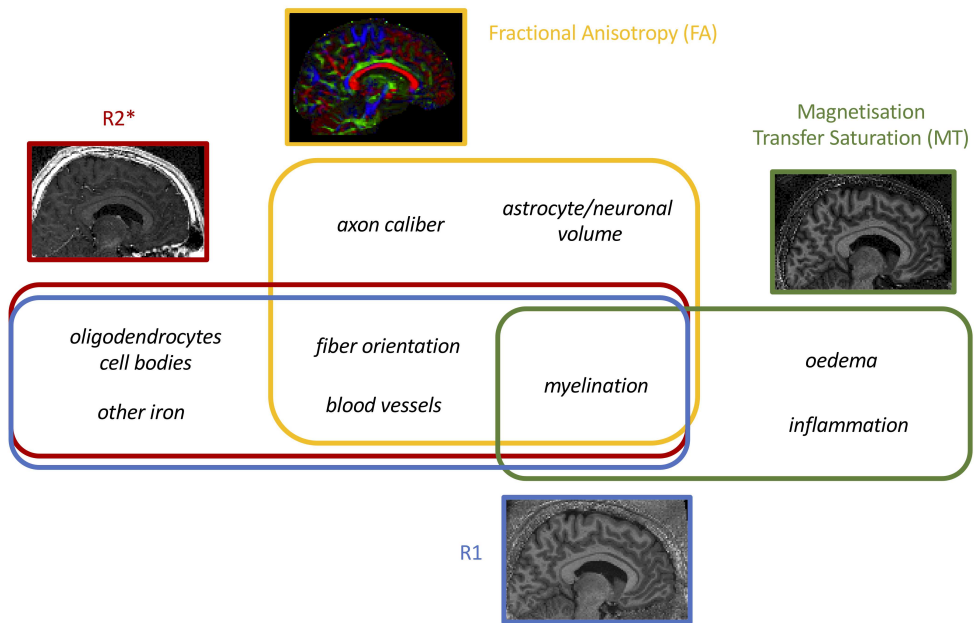


Figure 1: Each neuroimaging modality is sensitive, but not specific, to different features of the biological tissue. This study aimed to use multiple MR modalities that are sensitive to myelin, but measure different biophysical properties of white matter.

## 60 Methods

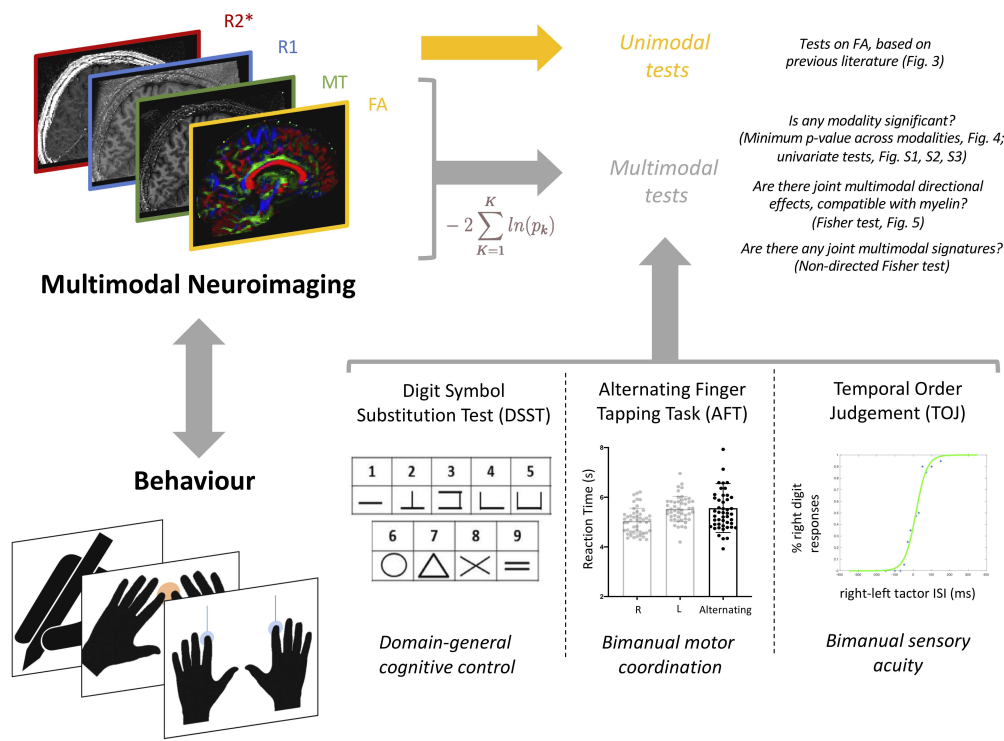


Figure 2: Study design and summary of MRI and behavioural data acquired.

61 **Participants.** Figure 2 summarises the study design. 50 healthy participants  
62 (25 female; aged 18-38 years, mean 26.2 years, median 26 years) underwent  
63 a single session of behavioural testing and MRI on the same day. As there is  
64 limited literature on the sample sizes needed to robustly detect cross-sectional  
65 correlations, our target sample size was based on previous work which had  
66 informed our hypotheses ( $n=20$  for DSST (Metzler-Baddeley et al., 2012),  $n=21$   
67 for AFT, as the average sample size in the studies reviewed by (Gooijers and

68 Swinnen, 2014), and n=26 for TOJ (Husain et al., 2011)). Studies reporting  
69 positive results may underestimate the necessary sample sizes (Button et al.,  
70 2013), so we doubled the sample size reported from the literature, thus bringing  
71 our sample size in line with a report recommending samples sizes between n=20  
72 and n=40 for studies on FA (De Santis et al., 2014).

73 All participants were self-assessed right-handed and their handedness was  
74 further assessed through the Edinburgh Handedness Inventory (Oldfield, 1971)  
75 (score range 60-100, mean 87.2, median 90). All participants were screened for  
76 MRI safety, received monetary compensation for their participation, and gave  
77 their informed consent to participate in this study. All study procedures followed  
78 the Declaration of Helsinki, and were reviewed and approved by the local ethics  
79 committee at the University of Oxford.

80 **Preregistration.** Details of the task data collection and analysis plans were pre-  
81 registered on the Open Science Framework website (full pre-registration available  
82 here: <https://osf.io/ar7zs/>). In brief, the pre-registration covered hypotheses  
83 and aims of the project, including which behavioural measures, MR metrics and  
84 regions of interest to use, while analytical details were decided separately after  
85 data collection.

86 We report here relevant text from the pre-registration: "Overall aim: testing  
87 whether previously reported correlations between behavioural measures and  
88 fractional anisotropy (FA) measures in long-range projections obtained using  
89 diffusion-weighted magnetic resonance imaging (dw-MRI) are related to indices  
90 of myelin content obtained using novel quantitative magnetic resonance imaging

91 (qMRI) protocols. To this end, we aim to replicate a sample of previous studies,  
92 and extend these FA/behaviour analyses to myelin qMRI/behaviour analyses".  
93 Specific brain/behaviour predictions were made for each task, listed in the  
94 analysis section below.

95 **Behavioural tasks.** A set of behavioural tasks was selected to build on prior  
96 studies reporting relationships between behaviour and WM microstructure.

97 The presence of FA-behaviour relationships has been particularly clear for the  
98 corpus callosum and for the cingulum. The cingulum has been often implicated  
99 in cognitive control (Bathelt et al., 2019), and cingulum FA has been found  
100 to strongly correlate with performance on neuropsychological tasks (Metzler-  
101 Baddeley et al., 2012). The corpus callosum, on the other hand, allows the  
102 nodes of the motor network in each hemisphere to communicate with one another,  
103 and both positive and negative relationships have been widely reported between  
104 callosal FA and various types of bimanual performance ((Johansen-Berg et al.,  
105 2007; Muetzel et al., 2008; Sullivan et al., 2001) and (Gooijers and Swinnen,  
106 2014) for a comprehensive review of callosal-bimanual behaviour relationships).

107 FA-behaviour relationships have also been thoroughly explored in behavioural  
108 paradigms beyond the motor system. As mentioned above, bimanual motor  
109 performance has been the subject of much literature, and so has bilateral sensory  
110 processing. In the visual domain, topographic organisation and visuospatial  
111 capacity have both been shown to relate to callosal microstructure (Saenz and  
112 Fine, 2010; Todorow et al., 2014). In the auditory domain, relationships have  
113 been established between perceptual acuity and WM microstructure, although

114 mostly in pathology (Husain et al., 2011; Lin et al., 2008; Wang et al.,  
115 2019). While there have been no previous studies on WM relationships with  
116 somatosensory acuity, it would be logical to expect a similar relationship between  
117 somatosensory perceptual acuity and microstructure of WM in relevant tracts.

118 Specifically, we assessed three task domains:

119 (1) testing for a relationship between callosal FA and bimanual motor  
120 performance using the Alternating Finger Tapping task aimed to directly replicate  
121 a series of previous studies (reviewed by (Gooijers and Swinnen, 2014) );

122 (2) testing for a relationship between cingulum FA and performance using the  
123 Digit Symbol Substitution Test (Metzler-Baddeley et al., 2012). Previous findings  
124 for this task were only reported in older adults (age range: 53 to 93, mean age:  
125 74 (Metzler-Baddeley et al., 2012)), accounting for confounding effects of age.  
126 Here, to maintain comparability to the other tasks studied, we tested a younger  
127 population.

128 (3) testing for a relationship between FA in somatosensory tracts and  
129 somatosensory perceptual acuity using the Temporal Order Judgement Task  
130 aimed to extend previous findings in the visual and auditory domain, to the  
131 sensory system.

132 These three tasks are described in detail below.

133 **Digit Symbol Substitution Test (DSST).** A paper-based Digit Symbol  
134 Substitution Test (DSST) was conducted as per [https://healthabc.nia.nih.gov/sites/default/files/dsst\\_0.pdf](https://healthabc.nia.nih.gov/sites/default/files/dsst_0.pdf). After training on substituting 10 digits for  
135 symbols, participants were asked to sequentially fill in the remaining 90 symbol-

137 digit boxes in 90 seconds.

138 **Analysis of the DSST.** The score was calculated as the total number of  
139 symbols filled in correctly by the end of the task. Two participants were identified  
140 as outliers ( $>3$  SD away from the mean) and thus excluded from further analyses.

141 **Alternating Finger Tapping (AFT) task.** The finger tapping task aimed to  
142 test the participants' bimanual coordination. The task was based on (Muetzel  
143 et al., 2008) and (Pelletier et al., 1993) and ran as follows: three blocks  
144 were repeated four times (the first one for training purposes): during the first  
145 block, participants were asked to tap their right index finger on a buttonbox  
146 (Current Designs, Inc., Philadelphia, PA) 30 times, as fast as they could (right  
147 monomotor condition); during the second block, participants were asked to  
148 tap their left index finger (left monomotor condition); during the third block,  
149 participants were asked to alternate between right and left index finger button  
150 presses (bimanual condition). For each block, after the 30 button presses were  
151 finished, the total elapsed time was fed back on the computer screen. The  
152 experimenter inspected the participant movement by eye to ensure they were  
153 correctly switching between fingers and that they were moving the finger rather  
154 than the hand. Participant posture and hand position was carefully kept constant  
155 throughout all blocks. One participant did not carry out the AFT due to a  
156 hardware problem.

157 **Analysis of the AFT task.** Alternating Finger Condition (AFC) duration was  
158 extracted, i.e. average total time needed for 30 taps on the alternating finger

159 condition (Muetzel et al., 2008). Two participants were identified as outliers (160  $>3$  SD away from the mean) and thus excluded from further analyses. Total 161 time needed for 30 taps on the monomotor conditions was used as a covariate 162 in group-level analyses, (Pelletier et al., 1993), together with age and gender.

163 **Temporal Order Judgement (TOJ) task.** The Temporal Order Judgement 164 (TOJ) task aimed to test participants' capacity to discriminate between two 165 closely timed tactile stimuli delivered to the fingertips. The task was based 166 on a previous investigation of the functional activity associated with such 167 behaviour (Kolasinski et al., 2016) and ran as follows. A PC running a 168 PsychoPy script delivered, via a USB 6501 card (National Instruments) and an 169 amplifier (Tactamp, Dancer Design), two asynchronous pulses to two vibrotactile 170 stimulators (also known as tactors, Dancer Design) positioned within holes in a 171 foam pad. The participant was asked to keep their hands relaxed on the foam 172 pad, with their index fingers gently lying on the tactors. A piece of cardboard 173 was used to block visual input from the tactors; similarly, headphones playing 174 low levels of pink noise were used to block the auditory input from the tactors. 175 Participants performed a two alternative forced choice (2AFC) task and were 176 asked to press on one of two foot pedals, depending on the side of the pulse 177 that they thought had come first. Participants were asked to respond within 2 178 seconds. If they did not respond within this time then no response was recorded 179 and a new trial was started. They were also instructed that if it was hard to 180 judge which pulse came first, they should just make their best guess. Intervals 181 between pulses ranged from 0 to 300 ms. The task featured a practice session

182 with 10 trials and a full session with 280 trials, for a total duration of roughly 12  
183 minutes.

184 **Analaysis of the TOJ task.** After trials with no response were discarded,  
185 the number of correct pedal responses were plotted as a function of inter-  
186 stimulation interval and a logistic regression was fitted to the data. At this  
187 stage, six participants were excluded as the logistic regression failed to fit the  
188 data correctly. The slope of the curve and the Just Noticeable Difference (JND)  
189 were used as key metrics of performance on the task (Kolasinski et al., 2016;  
190 Shore et al., 2005).

191 **MRI data collection.** Magnetic Resonance Imaging (MRI) data were collected  
192 with a 3.0-T Prisma Magnetom Siemens scanner, software version VE11C  
193 (Siemens Medical Systems, Erlangen, Germany). Participants were asked to  
194 keep their head still and to wear earplugs during scanning in order to reduce  
195 the impact of MRI-related noise. The sequences were collected as follows:  
196 T1-weighted structural imaging (T1w), resting-state fMRI (rs-fMRI), Multi-  
197 Parameter Mapping (MPM) and Diffusion-Weighted Imaging (DWI). MRI scan  
198 pre-processing, analysis and statistical comparisons were performed using FMRIB  
199 Software Library (FSL, v6.0), except for the MPM quantitative map estimation  
200 step which was carried out using the hMRI toolbox implemented in Matlab-based  
201 SPM, as described in (Tabelow et al., 2019).

202 The T1w sequence had a TR of 1900 ms, TE of 3.96 ms, a 1mm isotropic  
203 resolution and a large Field of View (FOV, 256 mm<sup>3</sup>) to allow for the nose

204 to be included in the image and thus facilitate neuronavigation later on in the  
205 paradigm. The sequence used GRAPPA with an acceleration factor of 2.

206 The diffusion-weighted Echo-planar imaging (EPI)sequence had TR=3070  
207 ms, TE=85 ms, FOV=204mm<sup>3</sup>, voxel size=1.5mm isotropic, multiband factor  
208 of 4. Diffusion scans were collected for two b-values (500 and 2000 s/mm<sup>2</sup>),  
209 over 281 directions. An additional 23 volumes were acquired at b=0, 15 in AP  
210 phase-encoding direction and 8 in the PA phase-encoding direction.

211 The MPM protocol (as per (Weiskopf et al., 2013)) included three multi-  
212 echo 3D FLASH (fast low-angle shot) scans with varying acquisition parameters,  
213 one RF transmit field map (B1+map) and one static magnetic (B0) field map  
214 scan, for a total acquisition time of roughly 22 minutes. To correct for inter-  
215 scan motion, position-specific receive coil sensitivity field maps, matched in FOV  
216 to the MPM scans, were calculated and corrected for (Papp et al., 2016). The  
217 three types of FLASH scans were designed to be predominantly T1-, PD-, or MT-  
218 weighted by changing the flip angle and the presence of a pre-pulse: 8 echoes were  
219 predominantly Proton Density-weighted (TR = 25ms; flip angle = 6 degrees;  
220 TE = 2.3-18.4ms), 8 echoes were predominantly T1-weighted (TR = 25ms;  
221 flip angle = 21 degrees; TE = 2.3-18.4ms) and 6 echoes were predominantly  
222 Magnetisation Transfer-weighted (MTw, TR = 25ms; flip angle = 6 degrees;  
223 TE = 2.3-13.8ms). For MTw scans, excitation was preceded by off-resonance  
224 Gaussian MT pulse of 4 ms duration, flip angle of 220 degrees, 2 kHz frequency  
225 offset from water resonance. All FLASH scans had 1 mm isotropic resolution and  
226 field of view (FOV) of 256x224x176 mm. The B1 map was acquired through  
227 an EPI-based sequence featuring spin and stimulated echoes (SE and STE) with

228 11 nominal flip angles, FOV of 192x192x256 mm and TR of 500 ms. The TE  
229 was 37.06 ms, and the mixing time was 33.8 ms. The B0 map was acquired to  
230 correct the B1+ map for distortions due to off-resonance effects. The B0 map  
231 sequence had a TR of 1020.0 ms, first TE of 10 ms, second TE of 12.46 ms, field  
232 of view (FOV) of 192x192x256 mm and read-out bandwidth of 260 Hz/pixel.

233 **MRI preprocessing.** A custom pipeline based on existing FSL tools (Smith  
234 et al., 2004) was developed for our diffusion sequence. The topup tool was  
235 run on average images of AP b0 volumes and PA b0 volumes. The resulting  
236 susceptibility-induced off-resonance field was used as an input for the eddy tool  
237 (Andersson and Sotiroopoulos, 2016), which was run with options optimised for  
238 multiband diffusion data to correct for eddy currents and subject movement. To  
239 generate Fractional Anisotropy (FA) maps, a diffusion tensor model was fit to  
240 each voxel through DTIFIT.

241 Magnetisation Transfer saturation (MT), R1 and R2\* quantitative maps were  
242 estimated through the hMRI toolbox (Tabelow et al., 2019), with default settings  
243 including ESTATICS modelling (Weiskopf et al., 2014). In order to register  
244 MPM volumes to FA volumes, we used the following steps. Boundary-Based  
245 Registration was used to calculate a DWI-to-T1w registration using preprocessed  
246 b0 images (with high tissue boundary contrast). A customised pipeline was used  
247 to apply the fslreorient2std tool to the MPM maps and register them to T1w  
248 space. At this stage, 1 participant was excluded as the MPM-derived maps were  
249 heavily corrupted due to movement artefacts; 1 participant was excluded due  
250 to lower quality signal in the MPM scan, which resulted in poor registration

251 with other modalities. Once registration matrices for MPM-T1w and DWI-T1w  
252 were calculated, they were inverted, concatenated and applied as needed to bring  
253 MPM volumes into DWI space with minimal interpolation. Registrations were  
254 assessed manually and one participant was excluded due to poor registration  
255 across all analyses.

256 **MRI analysis.** To bring all volumes into a common space, native FA volumes  
257 were skeletonised with Tract-Based Spatial Statistics (TBSS (Smith et al.,  
258 2006)), and the skeletonisation transforms were subsequently applied to MPM-  
259 to-DWI registered volumes. Group-level analyses were then conducted in skeleton  
260 space for all data.

261 All behavioural performance measures were normalised (through z-scoring,  
262 or rank-based inverse-normal transformation if not normally distributed) and  
263 correlations between MRI metrics and behaviour were assessed for each  
264 behavioural measure separately.

265 Relevant text from the preregistered analysis plan is as follows:

266 Cingulum and DSST: “We aim to replicate a reported relationship between  
267 [...] number of substituted digits in the Digit Substitution test and cingulum FA  
268 (Metzler-Baddeley et al., 2012) [...], and to extend the protocol to investigate  
269 qMRI [...] /behaviour relationships.”

270 Callosum and AFT: “We aim to replicate a reported relationship between  
271 callosal FA and AFC duration in the finger tapping task (Sullivan et al. 2001;  
272 Muetzel et al., 2008). We further aim to test for a relationship between myelin  
273 metrics in the corpus callosum and AFC duration”

274 Sensorimotor tracts and TOJ: “Performance on the temporal order judgement  
275 task is not associated with integrity of a single specific white matter tract, but  
276 rather with a set of tracts involving multiple sensorimotor areas. Accordingly, we  
277 plan to run exploratory analyses across the whole brain, testing for associations  
278 between JND/slope values and FA/qMRI.”

279 Covariates of age, sex, and performance on control tasks (unimanual finger  
280 tapping speed for the AFT, and visuomotor speed for DSST) were included.  
281 For each behavioural assay, voxelwise analyses were restricted to voxels within  
282 a predefined anatomical mask chosen from standard atlases included in FSL  
283 and based on the a priori hypotheses: a cingulum mask for DSST, a callosal  
284 mask for AFT and a mask of cortico-cortical and ascending sensorimotor tracts  
285 for TOJ. The masks were derived from the JHU ICBM-DTI-81 Atlas, the JHU  
286 White-Matter Tractography Atlas and the Human Sensorimotor Tracts Atlas,  
287 respectively.

288 Within these masks, analyses were conducted with voxelwise maps of FA,  
289 MT, R1 and R2\*. Voxelwise inference across these MRI modalities, testing  
290 for correlations between each MRI modality and behavioural measures, was  
291 performed using the Permutation Analysis of Linear Models (PALM) tool  
292 (Winkler et al., 2014). Cluster-wise inference was conducted to control familywise  
293 error over the image. A cluster-forming threshold of  $t > 1.7$  (equivalent to  $p < 0.05$ ,  
294 based on the degrees of freedom) was used in all instances, at the 5% familywise  
295 error level.

296 **Unimodal tests of FA.** For unimodal hypotheses on FA, we reported the  
297 univariate results for correlations between FA and behaviour.

298 **Multimodal tests.** For multimodal hypotheses, voxelwise inference using Non-  
299 Parametric Combination (NPC), as implemented in PALM (Winkler et al. 2016),  
300 was used to produce two types of inferences. (1) Correcting over modalities  
301 allowed us to ask whether *any individual modality* correlates with behaviour;  
302 (2) Combining over modalities allowed us to ask whether *any combination of*  
303 *modalities* correlates with behaviour.

304 For approach (1), we conducted cluster-wise inference on each modality  
305 separately, with familywise error controlled over the image and the  $K$  modalities.  
306 For each voxel, we reported the minimum image/modality-corrected cluster p-  
307 value across modalities.

308 For approach (2), combining evidence of effects over  $K$  modalities, we used  
309 Fisher's p-value combining method at each voxel:

$$- 2 \sum_{K=1}^K \ln(p_k) \quad (1)$$

310 With this approach, evidence can be assessed for either directional or non-  
311 directional effects: combining one-sided p-values (based on prior expected  
312 directions of effects) will test for directional effects; combining two-sided p-  
313 values will provide sensitivity to non-directional effects (i.e., combination of either  
314 direction) as well. Here, a directional Fisher test, testing for positive effects across  
315 all modalities, was used to test for putative myelin signatures.

316 **Simulation-based post-hoc power calculations for combined multimodal**  
317 **tests.** A comprehensive power analysis for cluster-wise inference that accounts  
318 for the spatially-varying dependence among imaging modalities is beyond the  
319 scope of this work. However, so as to provide a rough indication of power for  
320 future studies of multimodal microstructural imaging, we conducted univariate  
321 simulation-based power calculations for the combined multimodal (Fisher) tests.  
322 Pearson correlations for each modality-behaviour pair were recorded at the  
323 location of the peak voxel in the Fisher test inference map. In each simulation, a  
324 Gaussian random vector of behavioural and imaging values were generated with  
325 the specified correlation induced between the behaviour and each imaging value.  
326 We then tested whether the null hypothesis for each simulation would be rejected  
327 under a Fisher test with alpha set at 0.001. Power was then calculated as the  
328 percentage of tests rejecting the null hypothesis across all simulations. For each  
329 WM-behaviour correlation, power was calculated for samples sizes ranging from  
330 10 to 300 subjects. While this approach may be optimistic because of using a  
331 peak voxel to measure effect sizes, it probably is conservative since it represents  
332 power at a single voxel and does not reflect the sensitivity gained through cluster  
333 inference.

## 334 Results

335 We first used unimodal analyses to test for correlations between DWI-derived  
336 FA and behaviour, based on previously reported literature (Figure 3). No  
337 relationships were found between behaviour and FA within tracts of interest for  
338 either TOJ or DSST (TOJ: peak  $p_{corr}=0.08$ ; DSST: peak  $p_{corr}=0.49$ ). For AFT,  
339 a significant correlation was found between callosal FA and AFT performance  
340 (peak  $p_{corr}=0.016$ ).

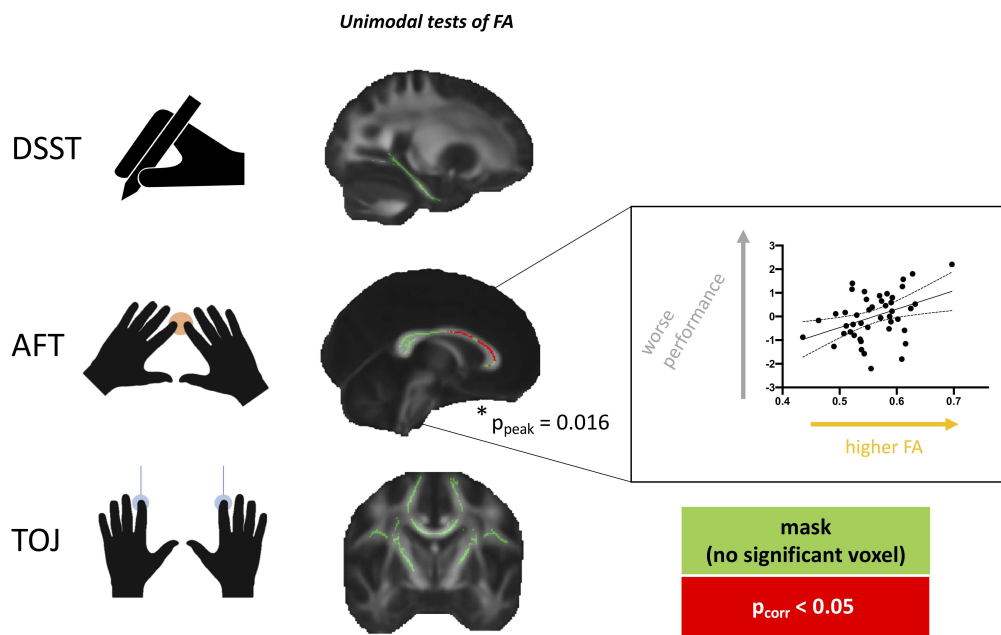


Figure 3: **FA and behaviour.** Unimodal relationships between FA and behaviour were tested across anatomical masks (shown in green) that were selected for each task. Results highlight that the Alternating Finger Tapping task (AFT), but not Temporal Order Judgement task (TOJ) and Digit Symbol Substitution Test (DSST) has a significant relationship with FA (red cluster shows voxels with corrected  $p$ -values below 0.05). Within that cluster, mean FA is extracted for each subject and plotted against performance in the scatterplot (with line of best fit and 95% confidence bands), that is for visual assessment of the correlation, rather than for statistical inference.

341 We then performed multimodal tests, testing whether *any individual* modality  
342 (FA, MT, R1 or R2\*) strongly correlated with behaviour (Figure 4), by  
343 considering p-values across both voxels and modalities for each WM-behaviour  
344 relationship. No relationships were found between behaviour and multimodal MRI  
345 metrics within tracts of interest for either TOJ or AFT (TOJ: peak  $p_{corr}=0.339$ ;  
346 or AFT: peak  $p_{corr}=0.09$ ). For DSST, a significant correlation was found between  
347 parahippocampal cingulum and DSST (peak  $p_{corr}=0.038$ ), driven entirely by R1  
348 (only modality with any voxel of  $p_{corr} < 0.05$ , Figure 4).

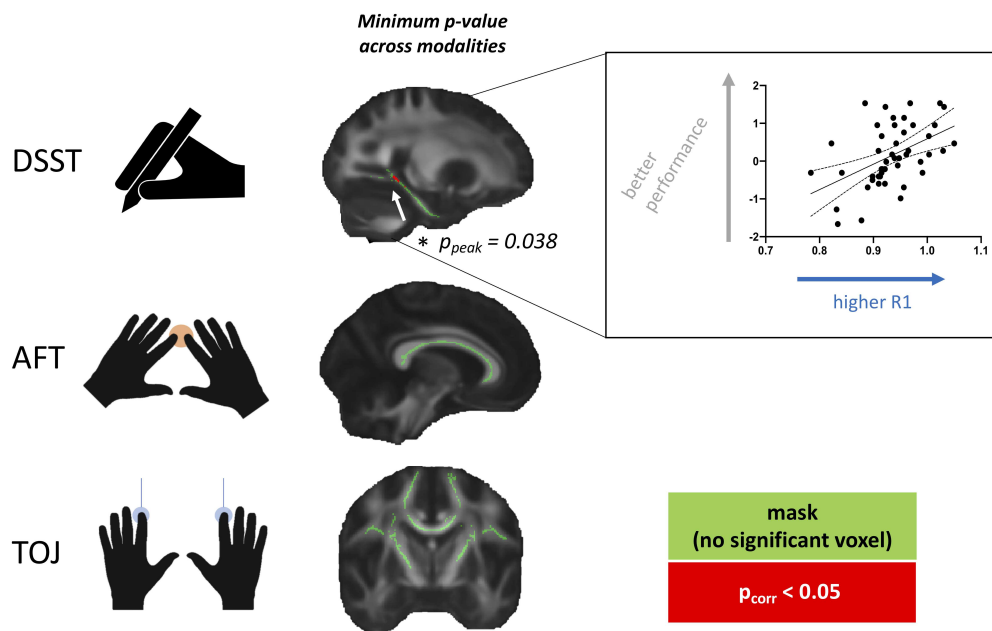


Figure 4: **Multimodal microstructural imaging and behaviour.** Multimodal relationships between behaviour and individual MRI metrics (FA, MT, R1 and R2\*) across Digit Symbol Substitution Test (DSST), Alternating Finger Tapping task (AFT) and Temporal Order Judgement task (TOJ). Only the DSST has a significant relationship with cingulum WM, driven by R1, when considering FWER-corrected p-values (red cluster shows voxels with corrected p-values below 0.05). Within that cluster, mean R1 is extracted for each subject and plotted against performance in the scatterplot (with line of best fit and 95% confidence bands), that is for visual assessment of the correlation, rather than for statistical inference.

349 While single-modality tests allow to identify strong correlations with a  
350 particular modality, they cannot identify combined trends across modalities,  
351 which can be particularly informative of the underlying biology. For instance,  
352 a positive trend across all modalities considered here (which are known to  
353 positively correlate with myelin content of the tissue) would indicate that tissue  
354 myelination may be related to behavioural performance. Likewise, trends in  
355 discordant directions could also be informative, as they could unveil multimodal

356 signatures related to other biological tissue properties such as vasculature and  
357 fiber orientation.

358 Fisher tests were used to detect combined multimodal trends between  
359 behavioural measures and MRI metrics (FA, MT, R1 and R2\*). With the usual  
360 (directed, positive) Fisher test (Figure 5, 2<sup>nd</sup> column), no relationships were  
361 found between behaviour and multimodal MRI metrics within tracts of interest  
362 (TOJ: peak  $p_{corr}=0.532$ ; AFT: peak  $p_{corr}=0.184$ ; DSST: peak  $p_{corr}=0.2$ ). With  
363 a non-directed Fisher test (results not shown), once again no relationships were  
364 found between behaviour and multimodal MRI metrics within tracts of interest.  
365 (TOJ: peak  $p_{corr}=0.82$ ; AFT: peak  $p_{corr}=0.11$ ; DSST: peak  $p_{corr}=0.29$ ) Taken  
366 together, these two tests argue against the presence of consistent multimodal  
367 microstructural signatures related to myelination or to other biological tissue  
368 properties.

369 The lack of a common microstructural signature is also apparent when  
370 considering the top 5<sup>th</sup> percentile t-statistics (Figure 5, 3<sup>rd</sup> column) and the  
371 t-statistics maps for each task (Figures S1, S2 and S3), where peaks are not  
372 consistent across modalities. This further confirms the negative Fisher tests, as  
373 there is no common trend across modalities within each group of WM-behaviour  
374 tests.

375 To aid future studies wishing to explore WM-behaviour correlations, and  
376 myelin-behaviour correlations in particular, we ran post-hoc simulation-based  
377 power analyses to identify the sample sizes needed to detect a combined  
378 multimodal effect through a Fisher test (Fig. 5, 4<sup>th</sup> column). Based on the  
379 observed effect sizes, we find that sample sizes needed to detect a myelin-

380 behaviour correlation across the 4 modalities in a directed Fisher test vary from  
381 190-200 participants for DSST, to 40-50 for AFT, to 60-70 for TOJ.

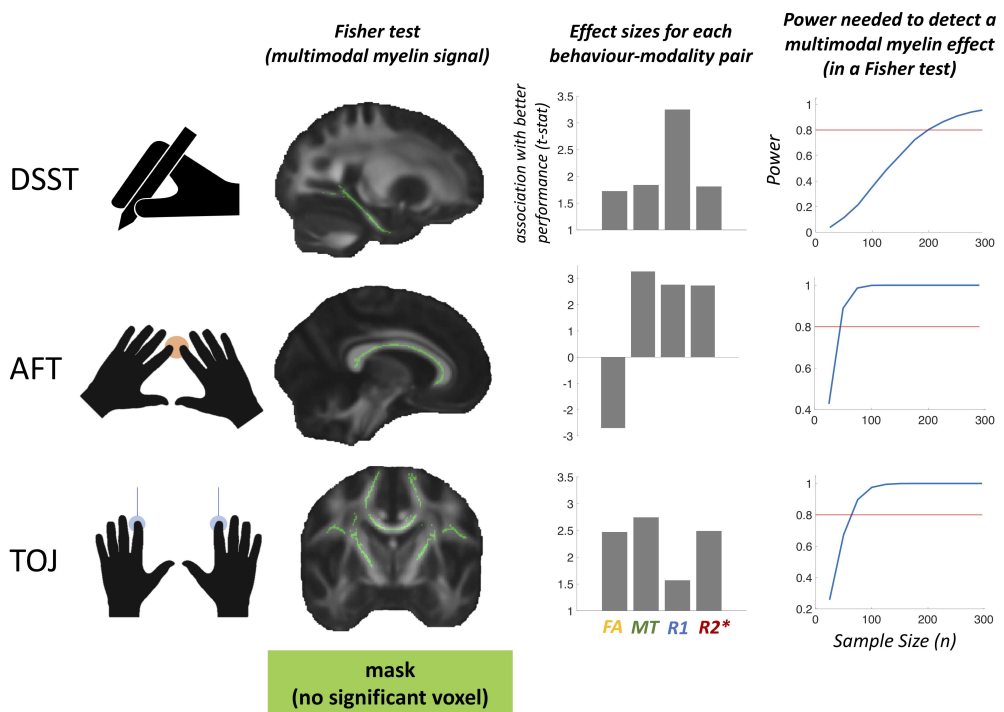


Figure 5: **Lack of evidence for combined multimodal signatures.** A Fisher test was used to search for multimodal microstructural signatures relating WM to behavior, but no significant effects were found (2<sup>nd</sup> column). Effect sizes are reported for each modality-behaviour correlation, as measured by the top 5% t-statistic within peak Fisher clusters. This analysis was carried out to provide a clear visualisation of peak effect size for each pair of MR modality and behaviour, rather than for statistical inference (3<sup>rd</sup> column). For each WM-behaviour correlation, we used a simulation-based approach to calculate sample sizes needed to reach 80% power (red line), given the observed effect sizes found in our pre-registered tests. Sample sizes needed to detect a combined multimodal effect vary from 190-200 participants for DSST, to 40-50 for AFT, to 60-70 for TOJ (4<sup>th</sup> column).

382 For completeness, we also report analyses of this dataset using conventional  
383 univariate approaches, considering each modality separately (Figures S1, S2

384 and S3) and not correcting across modalities. We find that if each modality-  
385 behaviour correlation was run as a separate analysis, each behaviour would show  
386 a correlation with at least one modality. Strikingly, different behaviours correlate  
387 most strongly with different modalities (DSST with R1 (Figure S1); AFT with  
388 FA and MT (Figure S2); TOJ with R2\* (Figure S3)), thus strengthening the  
389 evidence against a common microstructural signature across behaviours.

## 390 Discussion

391 Our first aim was to assess the robustness of relationships between white  
392 matter FA and behaviour across a range of behavioural tasks. We find a  
393 unimodal correlation between the structure of the corpus callosum FA and  
394 bimanual coordination, in accordance with previous literature (Bathelt et al.,  
395 2019; Johansen-Berg et al., 2007; Metzler-Baddeley et al., 2012; Muetzel et al.,  
396 2008; Sullivan et al., 2001). This confirms that individuals with lower callosal  
397 FA perform better in tasks requiring bimanual coordination. It also suggests that  
398 the extensive early literature on bimanual coordination and the corpus callosum  
399 (Gooijers and Swinnen, 2014) can be replicated, even with larger sample sizes  
400 and recent preprocessing pipelines.

401 However, a robust relationship between FA and behaviour was identified  
402 in only one out of three tasks considered here. This can be due to several  
403 reasons. One possible explanation is that effect sizes inferred from previous  
404 studies might be overinflated due to publication bias (Turner et al., 2008) and  
405 under-powered analyses (Button et al., 2013). However, it is worth noting that,  
406 of the three tasks considered here, only the FA-AFT experiment, which did  
407 successfully identify a FA-behaviour relationship, was a direct replication of a  
408 previous testing protocol. The other two tasks were designed as conceptual  
409 replications or extensions, but did not precisely replicate experimental conditions  
410 and analysis steps. For instance, our analyses employed Tract-Based Spatial  
411 Statistics (Smith et al., 2006), as well as recently developed preprocessing tools  
412 (Andersson and Sotiroopoulos, 2016), both of which differed from some of the

413 studies we based our hypotheses on (Metzler-Baddeley et al., 2012). While our  
414 aim was not to perfectly replicate analyses from previous papers, it is possible that  
415 differences in preprocessing may be driving discrepancies between our FA results  
416 and the results from previous studies. In summary, the relationships between FA  
417 and behaviour that have been established may be robust and replicable, but the  
418 experimental and analytic conditions under which they occur needs clarification.

419 A second aim of the present study was to probe whether multimodal MR can  
420 provide useful insights on WM-behaviour relationships. We find that this is the  
421 case for at least one of the WM-behaviour relationships we tested: R1 correlates  
422 with DSST performance, such that individuals with higher R1 perform better in  
423 the DSST task requiring cognitive control. Higher R1 could reflect greater myelin,  
424 oligodendrocytes, vasculature or other iron-rich tissue components. In this case,  
425 multimodal analysis allowed identification of a WM-behaviour relationship that  
426 would have not been detected by an analysis focused on FA in isolation. This  
427 confirms that there is value in multimodal imaging, as some modalities may be  
428 more sensitive to the presence of a relationship than others.

429 A third aim was to test whether there are common multimodal microstructural  
430 patterns in WM-behaviour relationships, which may provide insights into the  
431 underlying biology. We fail to find robust evidence for multimodal effects and  
432 cross-modality signatures. Rather, we find that effect sizes and directionality of  
433 effect in the relationship between each modality and each behaviour are highly  
434 heterogeneous. This means that MR modalities in each tract not only show  
435 heterogeneity in how they relate to the same behaviour, but there is also variation  
436 as a function of which tract-behaviour correlation is being considered.

437 A key insight from the study is therefore that the relationship between WM  
438 and behaviour is highly varied. Given that each modality has a specific pattern of  
439 sensitivity to the underlying biology (Figure 1), the results suggest that different  
440 aspects of WM biology may be driving different WM-behaviour correlations.  
441 There are two prominent sources of biological heterogeneity in white matter,  
442 which are likely relevant to the results in this study.

443 One driver of heterogeneity may be at the level of myelination. We selected  
444 metrics that were all sensitive to the amount of myelin in an imaging voxel  
445 (Figure 1), predicting that if myelination were responsible for WM-behaviour  
446 relationships, a common multimodal pattern across all relationships would be  
447 identified. Such patterns were not found, arguing against myelination as a  
448 common driver. However, such reasoning might be overly simple-minded.  
449 Histological studies have increasingly highlighted the heterogeneity of features  
450 in the myelinated axon, which can vary independently of each other (Almeida  
451 and Lyons, 2017). For instance, we know that Nodes of Ranvier, myelin  
452 sheath thickness, myelin sheath length, and number of myelin sheaths, can all  
453 independently affect an axon's physiological properties, which one would expect,  
454 in turn, to shape behaviour (Kaller et al., 2017). Varying these features might  
455 have differing effects on the overall amount of myelin in a given voxel meaning  
456 that the imaging metrics used might not be equally sensitive to all relevant  
457 features of the myelinated axon.

458 A second important driver of heterogeneity is non-myelin features of WM.  
459 As exemplified in Figure 1, while all sequences we used are sensitive to myelin,  
460 some are also sensitive to fiber orientation and neuronal volume (FA), and some

461 are sensitive to iron and vasculature (R1 and R2\*). Therefore, one possible  
462 interpretation of the data is that the relationship between AFT performance  
463 and the corpus callosum is highly influenced by fiber orientation, whereas the  
464 relationship between the DSST performance and the cingulum is shaped by  
465 vasculature. Previous studies highlighted that both fiber orientation (Chang  
466 et al., 2017; Wedeen et al., 2005) and vasculature (Licht et al., 2011; Rhyu  
467 et al., 2010; Thomas et al., 2016) are important for brain function, and our data  
468 thus draw further attention to the fact that these factors may be influential in  
469 WM-behaviour relationships.

470 These two factors combined may explain why there is no single aspect of  
471 WM that drives behaviour. Rather, our findings confirm that heterogeneity at  
472 the cellular level is reflected in variation in the relationship between neuroimaging  
473 markers and behaviour. Importantly, this emphasizes that there is no single  
474 modality or single combination of modalities which is optimal to study WM-  
475 behaviour relationships. In this respect, our study poses practical limits to the  
476 possibility of developing a one-size-fits-all approach to the investigation of white  
477 matter-behaviour relationships, due to their inherent diversity.

478 While this heterogeneity means it is not straightforward to predict which MR  
479 modality is best suited for each type of WM investigation, it also suggests that  
480 multimodal studies of WM should tailor their MR sequence protocols and analyses  
481 pipelines to privilege markers and statistical approaches that can test and compare  
482 biologically-grounded models. For example, with an appropriate acquisition  
483 sequence and a joint multimodal statistical framework, one might be able to test  
484 whether a given WM-behaviour correlation is driven by myelination, vasculature

485 (Thomas et al., 2016), or connectivity (Sui et al., 2014). Such approaches are  
486 most likely to generate further insights into WM-behaviour relationships in the  
487 future.

488 One key limitation of the study is that the results cannot disentangle to  
489 what extent differences between WM tracts contribute to the observed diversity  
490 of WM-behaviour relationships. One could argue, for example, that our results  
491 demonstrate that FA is more important for WM-behaviour relationships involving  
492 the corpus callosum, whereas R1 is more important for understanding the  
493 cingulum, while MT/R2\* are more important in investigations of the corticospinal  
494 tract. Because each of the behaviours we selected relates to a different WM  
495 tract, it is impossible to disentangle whether different kinds of behaviours are  
496 most strongly driven by different microstructural patterns, or whether there is  
497 neuroanatomical heterogeneity in the importance of different microstructural  
498 features of each tract. Although both are likely to matter, further studies relating  
499 individual tracts to multiple behaviours are required.

500 Moreover, an additional limitation of the study lies in the extent to which  
501 it was pre-registered. While our pre-registration covered hypotheses and aims,  
502 including behavioural measures, MR metrics and regions of interest, it is now  
503 increasingly being acknowledged that many analytical choices in neuroimaging  
504 can have a large influence on the final results (Nichols et al., 2017; Pervaiz  
505 et al., 2020), and are thus crucial for confirmatory analyses. Therefore, we  
506 recommend future studies to include sample size and details of their preprocessing  
507 and statistical modelling in their pre-registrations when appropriate.

508 The results also hold useful lessons for statistical aspects of future multimodal

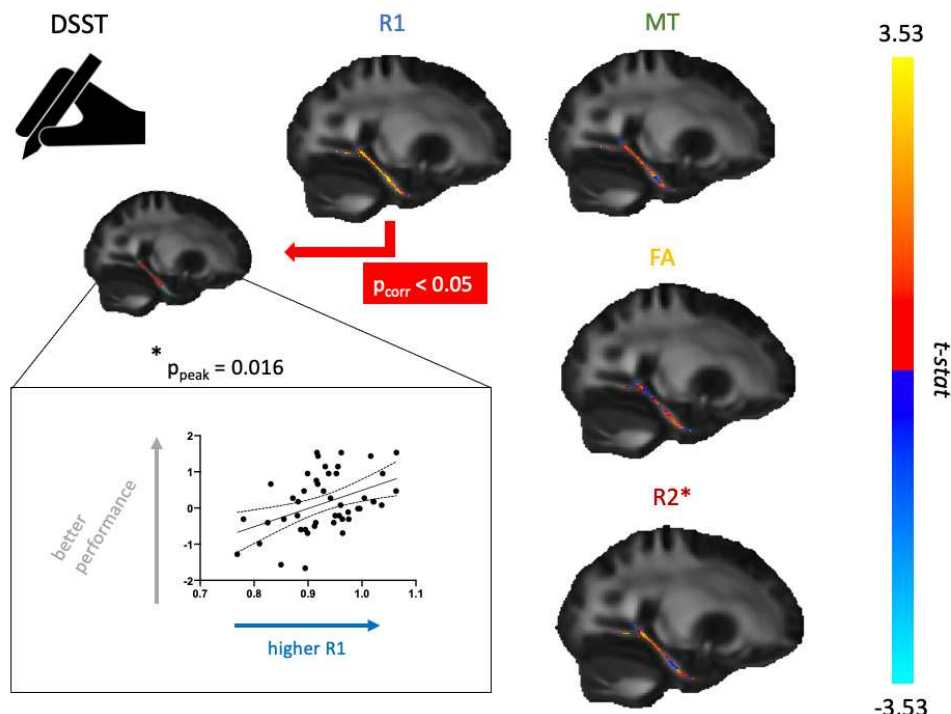
509 studies of WM. WM-behaviour correlations often have small effect sizes, and  
510 in our results we find that these effects are sometimes not detected when  
511 multiple hypotheses are tested concurrently. Testing for effects across modalities  
512 increases the false discovery rate proportionally to the number of modalities  
513 tested, and thus needs to be adequately corrected for in order to reach appropriate  
514 interpretations (Winkler et al., 2016). However, while multiple comparison  
515 correction has long been the gold standard statistical advice, multimodal brain  
516 imaging studies often do not report whether, and if so, how, correction for  
517 multiple comparisons was carried out (Bezukladova et al., 2020; Winston et al.,  
518 2020). Surprisingly, even gold standard guidelines in the field like COBIDAS  
519 do not report best practices for statistical reporting in multimodal imaging  
520 (Nichols et al., 2017), and many packages that support multi-modality statistical  
521 testing do not allow joint statistical tests, thus leaving room for needless analytic  
522 flexibility. Our results suggest there is a need for increased transparency in  
523 reporting of multimodal statistics, which statistical guidelines on multimodal  
524 imaging might facilitate in the future. In this respect, our results also add weight  
525 to previous calls to pre-register the modalities to be used in a given analysis  
526 (Picciotto, 2018), and to report all tested modalities in publications.

527 This aspect of statistics in multimodal studies also needs to be taken into  
528 account when assessing the power of a given analysis. When modalities are  
529 analysed separately, multimodal studies require multiple statistical tests across  
530 modalities. Therefore, for the same effect size, a study analysing multiple  
531 modalities may need more subjects to achieve the same power, and it is important  
532 to take this into account in power analyses. We thus recommend using larger

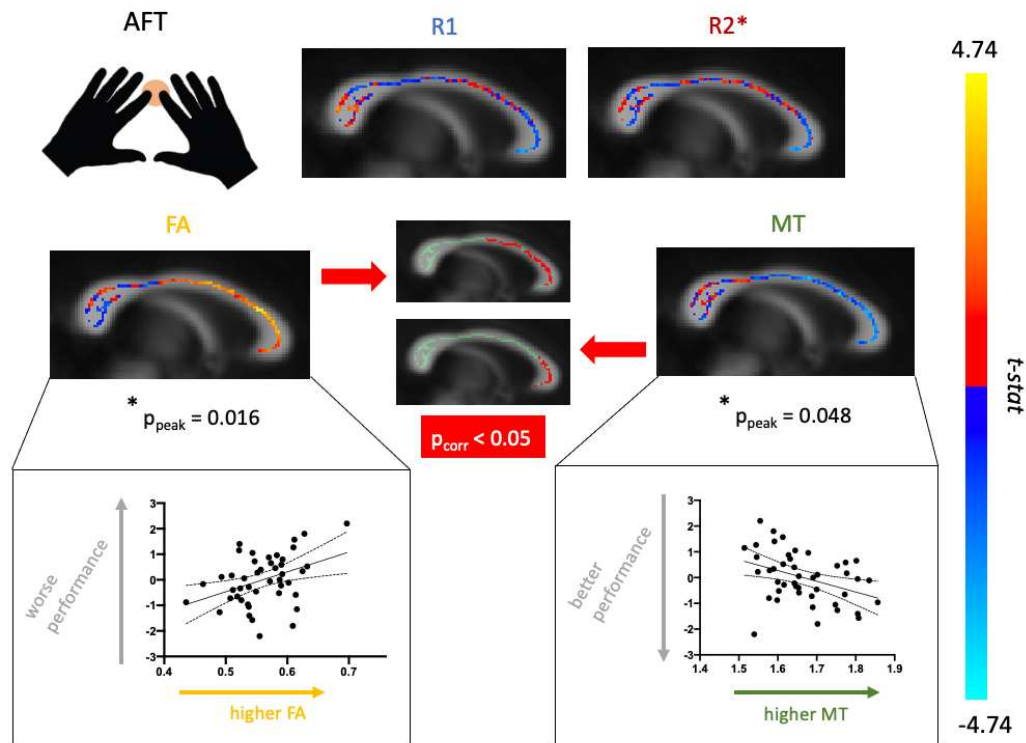
533 sample sizes for multimodal compared to unimodal studies. Alternatively, another  
534 solution is to use non-parametric multivariate tests (Winkler et al., 2014, 2016)  
535 and/or dimensionality reduction techniques (Groves et al., 2011; Sui et al., 2014),  
536 in scenarios where multimodal data are available but the data set size is only  
537 powered for unimodal tests. While there is little literature on multimodal power  
538 analyses for cross-sectional studies using microstructural imaging, our results  
539 indicate that sample sizes of 40 to 200 may be required to detect joint multimodal  
540 effects through non-parametric multivariate tests.

541 In conclusion, these results highlight a broad heterogeneity in white matter's  
542 relationship with behaviour. They also underscore the added value of multimodal  
543 imaging approaches, as different neuroimaging modalities might be best suited  
544 to detect different WM-behavior relationships. However, this added value needs  
545 to be weighed carefully against the need for more power and/or dimensionality  
546 reduction approaches in multimodal studies. Finally, the results effectively limit  
547 the possibility of developing a one-size-fits-all approach to study white matter,  
548 and suggest that different aspects of WM biology may be driving different WM-  
549 behaviour correlations.

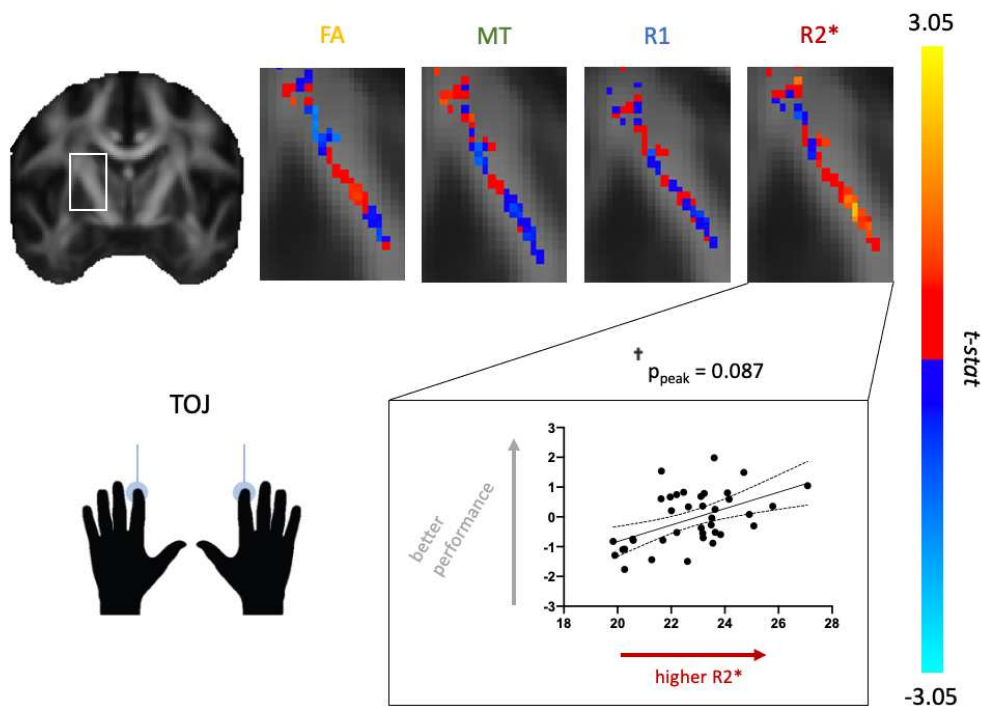
## 550 Supplementary Results



Supplementary Figure 1: **Correlation between DSST performance and cingulum microstructure, reported as univariate results.** For each modality, unthresholded  $t$ -statistics are visualized according the colour bar (right). For R1 only, a cluster of voxels survived the threshold of  $p < 0.05$ . Average R1 values within that cluster are shown against performance score in the scatterplot (with line of best fit and 95% confidence bands), which is presented for visualisation and is not used for statistical inference.



Supplementary Figure 2: **Correlation between AFT and callosal microstructure, reported as univariate results.** For each modality, unthresholded t-statistics are visualized according the colour bar (right). For FA and MT, clusters of voxels survived the threshold of  $p < 0.05$ . Average FA/MT values within that cluster are shown against performance score in the scatterplots (with line of best fit and 95% confidence bands), which are presented for visualisation and are not used for statistical inference.



Supplementary Figure 3: **Correlation between TOJ performance and CST microstructure, reported as univariate results.** For each modality, unthresholded t-statistics are visualized according to the colour bar (right). For  $R2^*$  only, a cluster of voxels reached  $p=0.087$ . Average  $R2^*$  values within that cluster are shown against performance score in the scatterplot (with line of best fit and 95% confidence bands), which is presented for visualisation and is not used for statistical inference.

## 551 **Acknowledgements**

552 We are grateful to Ilona Lipp and Kate Watkins for their input on the manuscript.  
553 We thank Claudia Metzler-Baddeley for providing additional details on her  
554 previous experiments, which helped guide the DSST-Cingulum analyses. We  
555 would like to thank Juliet Semple, Nicola Aikin and Sebastian Rieger for their  
556 technical support and help with scanning participants; and Matthew Webster for  
557 wide-ranging help from IT to statistical issues. We acknowledge the IT-related  
558 support provided by David Flitney and Duncan Mortimer throughout the project.

## 559 **Data Availability Statement**

560 Data used in this study is only available upon request due to data protection  
561 considerations.

## 562 **Funding**

563 This work was supported by a PhD Studentship awarded to AL from the  
564 Wellcome Trust (109062/Z/15/Z) and by a Principal Research Fellowship  
565 from the Wellcome Trust to HJB (110027/Z/15/Z). CJS holds a Sir Henry  
566 Dale Fellowship, funded by the Wellcome Trust and the Royal Society  
567 (102584/Z/13/Z). OJW was funded by the Erasmus+ Programme by the  
568 European Commission. NE is a Wellcome Trust Doctoral student in Neuroscience  
569 at the University of Oxford [203730/Z/16/Z]. AJ was funded by the Dunhill

570 Medical Trust (RPGF1810/93). The project was supported by the NIHR Oxford  
571 Health Biomedical Research Centre and the NIHR Oxford Biomedical Research  
572 Centre. The Wellcome Centre for Human Neuroimaging and the Wellcome  
573 Centre for Integrative Neuroimaging are supported by core funding from the  
574 Wellcome Trust [203147/Z/16/Z and 203139/Z/16/Z].

## 575 References

576 Almeida, R. G. and Lyons, D. A. (2017). On myelinated axon plasticity  
577 and neuronal circuit formation and function. *Journal of Neuroscience*,  
578 37(42):10023–10034.

579 Andersson, J. L. and Sotiroopoulos, S. N. (2016). An integrated approach to  
580 correction for off-resonance effects and subject movement in diffusion mr  
581 imaging. *Neuroimage*, 125:1063–1078.

582 Bathelt, J., Johnson, A., Zhang, M., and Astle, D. E. (2019). The cingulum  
583 as a marker of individual differences in neurocognitive development. *Scientific  
584 reports*, 9(1):2281.

585 Bezukladova, S., Tuisku, J., Matilainen, M., Vuorimaa, A., Nylund, M.,  
586 Smith, S., Sucksdorff, M., Mohammadian, M., Saunavaara, V., Laaksonen,  
587 S., et al. (2020). Insights into disseminated ms brain pathology with  
588 multimodal diffusion tensor and pet imaging. *Neurology-Neuroimmunology  
589 Neuroinflammation*, 7(3).

590 Boekel, W., Wagenmakers, E.-J., Belay, L., Verhagen, J., wn, S., and Forstmann,  
591 B. U. (2015). A purely confirmatory replication study of structural brain-  
592 behavior correlations. *Cortex*, 66:115–133.

593 Button, K. S., Ioannidis, J. P., Mokrysz, C., Nosek, B. A., Flint, J., Robinson,  
594 E. S., and Munafò, M. R. (2013). Power failure: why small sample size

595 undermines the reliability of neuroscience. *Nature Reviews Neuroscience*,  
596 14(5):365.

597 Chang, E. H., Argyelan, M., Aggarwal, M., Chandon, T.-S. S., Karlsgodt, K. H.,  
598 Mori, S., and Malhotra, A. K. (2017). The role of myelination in measures  
599 of white matter integrity: combination of diffusion tensor imaging and two-  
600 photon microscopy of clarity intact brains. *Neuroimage*, 147:253–261.

601 De Santis, S., Drakesmith, M., Bells, S., Assaf, Y., and Jones, D. K. (2014). Why  
602 diffusion tensor mri does well only some of the time: variance and covariance  
603 of white matter tissue microstructure attributes in the living human brain.  
604 *Neuroimage*, 89:35–44.

605 Deloire-Grassin, M., Brochet, B., Quesson, B., Delalande, C., Dousset, V.,  
606 Canioni, P., and Petry, K. (2000). In vivo evaluation of remyelination in rat  
607 brain by magnetization transfer imaging. *Journal of the neurological sciences*,  
608 178(1):10–16.

609 Dousset, V., Brochet, B., Vital, A., Gross, C., Benazzouz, A., Boullerne, A.,  
610 Bidabe, A.-M., Gin, A.-M., and Caille, J.-M. (1995). Lysolecithin-induced  
611 demyelination in primates: preliminary in vivo study with mr and magnetization  
612 transfer. *American journal of neuroradiology*, 16(2):225–231.

613 Dousset, V., Grossman, R. I., Ramer, K. N., Schnall, M. D., Young, L. H.,  
614 Gonzalez-Scarano, F., Lavi, E., and Cohen, J. A. (1992). Experimental  
615 allergic encephalomyelitis and multiple sclerosis: lesion characterization with  
616 magnetization transfer imaging. *Radiology*, 182(2):483–491.

617 Farquharson, S., Tournier, J.-D., Calamante, F., Fabinyi, G., Schneider-Kolsky,  
618 M., Jackson, G. D., and Connelly, A. (2013). White matter fiber tractography:  
619 why we need to move beyond dti. *Journal of neurosurgery*, 118(6):1367–1377.

620 Fünfschilling, U., Supplie, L. M., Mahad, D., Boretius, S., Saab, A. S., Edgar,  
621 J., Brinkmann, B. G., Kassmann, C. M., Tzvetanova, I. D., Möbius, W., et al.  
622 (2012). Glycolytic oligodendrocytes maintain myelin and long-term axonal  
623 integrity. *Nature*, 485(7399):517.

624 Gibson, E. M., Geraghty, A. C., and Monje, M. (2018). Bad wrap: Myelin  
625 and myelin plasticity in health and disease. *Developmental neurobiology*,  
626 78(2):123–135.

627 Gooijers, J. and Swinnen, S. (2014). Interactions between brain structure and  
628 behavior: the corpus callosum and bimanual coordination. *Neuroscience &*  
629 *Biobehavioral Reviews*, 43:1–19.

630 Groves, A. R., Beckmann, C. F., Smith, S. M., and Woolrich, M. W.  
631 (2011). Linked independent component analysis for multimodal data fusion.  
632 *Neuroimage*, 54(3):2198–2217.

633 Heath, F., Hurley, S. A., Johansen-Berg, H., and Sampaio-Baptista, C. (2018).  
634 Advances in noninvasive myelin imaging. *Developmental Neurobiology*,  
635 78(2):136–151.

636 Husain, F. T., Medina, R. E., Davis, C. W., Szymko-Bennett, Y., Simonyan,  
637 K., Pajor, N. M., and Horwitz, B. (2011). Neuroanatomical changes due

638 to hearing loss and chronic tinnitus: a combined vbm and dti study. *Brain*  
639 *research*, 1369:74–88.

640 Johansen-Berg, H. (2010). Behavioural relevance of variation in white matter  
641 microstructure. *Current opinion in neurology*, 23(4):351–358.

642 Johansen-Berg, H., Della-Maggiore, V., Behrens, T. E., Smith, S. M., and Paus,  
643 T. (2007). Integrity of white matter in the corpus callosum correlates with  
644 bimanual co-ordination skills. *Neuroimage*, 36:T16–T21.

645 Kaller, M. S., Lazari, A., Blanco-Duque, C., Sampaio-Baptista, C., and Johansen-  
646 Berg, H. (2017). Myelin plasticity and behaviour?connecting the dots. *Current*  
647 *opinion in neurobiology*, 47:86–92.

648 Kolasinski, J., Makin, T. R., Logan, J. P., Jbabdi, S., Clare, S., Stagg, C. J.,  
649 and Johansen-Berg, H. (2016). Perceptually relevant remapping of human  
650 somatotopy in 24 hours. *Elife*, 5:e17280.

651 Langkammer, C., Krebs, N., Goessler, W., Scheurer, E., Ebner, F., Yen, K.,  
652 Fazekas, F., and Ropele, S. (2010). Quantitative mr imaging of brain iron: a  
653 postmortem validation study. *Radiology*, 257(2):455–462.

654 Lazari, A., Koudelka, S., and Sampaio-Baptista, C. (2018). Experience-  
655 related reductions of myelin and axon diameter in adulthood. *Journal of*  
656 *neurophysiology*, 120(4):1772–1775.

657 Lazari, A. and Lipp, I. (2020). Can mri measure myelin? systematic review,

658 qualitative assessment, and meta-analysis of studies validating microstructural  
659 imaging with myelin histology. *bioRxiv*.

660 Licht, T., Goshen, I., Avital, A., Kreisel, T., Zubedat, S., Eavri, R., Segal,  
661 M., Yirmiya, R., and Keshet, E. (2011). Reversible modulations of neuronal  
662 plasticity by vegf. *Proceedings of the National Academy of Sciences*,  
663 108(12):5081–5086.

664 Lin, Y., Wang, J., Wu, C., Wai, Y., Yu, J., and Ng, S. (2008). Diffusion tensor  
665 imaging of the auditory pathway in sensorineural hearing loss: changes in radial  
666 diffusivity and diffusion anisotropy. *Journal of Magnetic Resonance Imaging: An Official Journal of the International Society for Magnetic Resonance in Medicine*, 28(3):598–603.

669 Lutti, A., Dick, F., Sereno, M. I., and Weiskopf, N. (2014). Using high-resolution  
670 quantitative mapping of r1 as an index of cortical myelination. *Neuroimage*,  
671 93:176–188.

672 Metzler-Baddeley, C., Jones, D. K., Steventon, J., Westacott, L., Aggleton,  
673 J. P., and O'Sullivan, M. J. (2012). Cingulum microstructure predicts cognitive  
674 control in older age and mild cognitive impairment. *Journal of Neuroscience*,  
675 32(49):17612–17619.

676 Muetzel, R. L., Collins, P. F., Mueller, B. A., Schissel, A. M., Lim, K. O.,  
677 and Luciana, M. (2008). The development of corpus callosum microstructure  
678 and associations with bimanual task performance in healthy adolescents.  
679 *Neuroimage*, 39(4):1918–1925.

680 Nave, K.-A. (2010). Myelination and support of axonal integrity by glia. *Nature*,  
681 468(7321):244.

682 Nichols, T. E., Das, S., Eickhoff, S. B., Evans, A. C., Glatard, T., Hanke, M.,  
683 Kriegeskorte, N., Milham, M. P., Poldrack, R. A., Poline, J.-B., et al. (2017).  
684 Best practices in data analysis and sharing in neuroimaging using mri. *Nature  
neuroscience*, 20(3):299.

686 Oldfield, R. C. (1971). The assessment and analysis of handedness: the edinburgh  
687 inventory. *Neuropsychologia*, 9(1):97–113.

688 Papp, D., Callaghan, M. F., Meyer, H., Buckley, C., and Weiskopf, N.  
689 (2016). Correction of inter-scan motion artifacts in quantitative r1 mapping by  
690 accounting for receive coil sensitivity effects. *Magnetic resonance in medicine*,  
691 76(5):1478–1485.

692 Pelletier, J., Habib, M., Lyon-Caen, O., Salamon, G., Poncet, M., and Khalil,  
693 R. (1993). Functional and magnetic resonance imaging correlates of callosal  
694 involvement in multiple sclerosis. *Archives of Neurology*, 50(10):1077–1082.

695 Pervaiz, U., Vidaurre, D., Woolrich, M. W., and Smith, S. M. (2020). Optimising  
696 network modelling methods for fmri. *Neuroimage*, 211:116604.

697 Picciotto, M. (2018). Analytical transparency and reproducibility in human  
698 neuroimaging studies.

699 Rhyu, I., Bytheway, J., Kohler, S., Lange, H., Lee, K., Boklewski, J., McCormick,  
700 K., Williams, N., Stanton, G., Greenough, W., et al. (2010). Effects of aerobic

701 exercise training on cognitive function and cortical vascularity in monkeys.

702 *Neuroscience*, 167(4):1239–1248.

703 Roberts, R. E., Anderson, E. J., and Husain, M. (2013). White matter

704 microstructure and cognitive function. *The Neuroscientist*, 19(1):8–15.

705 Saenz, M. and Fine, I. (2010). Topographic organization of v1 projections

706 through the corpus callosum in humans. *Neuroimage*, 52(4):1224–1229.

707 Sampaio-Baptista, C. and Johansen-Berg, H. (2017). White matter plasticity in

708 the adult brain. *Neuron*, 96(6):1239–1251.

709 Shore, D. I., Gray, K., Spry, E., and Spence, C. (2005). Spatial modulation of

710 tactile temporal-order judgments. *Perception*, 34(10):1251–1262.

711 Smith, S. M., Jenkinson, M., Johansen-Berg, H., Rueckert, D., Nichols, T. E.,

712 Mackay, C. E., Watkins, K. E., Ciccarelli, O., Cader, M. Z., Matthews, P. M.,

713 et al. (2006). Tract-based spatial statistics: voxelwise analysis of multi-subject

714 diffusion data. *Neuroimage*, 31(4):1487–1505.

715 Smith, S. M., Jenkinson, M., Woolrich, M. W., Beckmann, C. F., Behrens,

716 T. E., Johansen-Berg, H., Bannister, P. R., De Luca, M., Drobniak, I., Flitney,

717 D. E., et al. (2004). Advances in functional and structural mr image analysis

718 and implementation as fsl. *Neuroimage*, 23:S208–S219.

719 Steadman, P. E., Xia, F., Ahmed, M., Mocle, A. J., Penning, A. R., Geraghty,

720 A. C., Steenland, H. W., Monje, M., Josselyn, S. A., and Frankland, P. W.

721 (2019). Disruption of oligodendrogenesis impairs memory consolidation in  
722 adult mice. *Neuron*.

723 Stolp, H., Ball, G., So, P.-W., Tournier, J.-D., Jones, M., Thornton, C.,  
724 and Edwards, A. (2018). Voxel-wise comparisons of cellular microstructure  
725 and diffusion-mri in mouse hippocampus using 3d bridging of optically-clear  
726 histology with neuroimaging data (3d-bond). *Scientific reports*, 8(1):1–12.

727 Stüber, C., Morawski, M., Schäfer, A., Labadie, C., Wähnert, M., Leuze, C.,  
728 Streicher, M., Barapatre, N., Reimann, K., Geyer, S., et al. (2014). Myelin and  
729 iron concentration in the human brain: a quantitative study of mri contrast.  
730 *Neuroimage*, 93:95–106.

731 Sui, J., Huster, R., Yu, Q., Segall, J. M., and Calhoun, V. D. (2014). Function–  
732 structure associations of the brain: evidence from multimodal connectivity and  
733 covariance studies. *Neuroimage*, 102:11–23.

734 Sullivan, E. V., Rosenbloom, M. J., Desmond, J. E., and Pfefferbaum, A. (2001).  
735 Sex differences in corpus callosum size: relationship to age and intracranial size.  
736 *Neurobiology of aging*, 22(4):603–611.

737 Sun, H., Walsh, A. J., Lebel, R. M., Blevins, G., Catz, I., Lu, J.-Q., Johnson,  
738 E. S., Emery, D. J., Warren, K. G., and Wilman, A. H. (2015). Validation  
739 of quantitative susceptibility mapping with perls' iron staining for subcortical  
740 gray matter. *Neuroimage*, 105:486–492.

741 Tabelow, K., Balteau, E., Ashburner, J., Callaghan, M. F., Draganski, B., Helms,

742 G., Kherif, F., Leutritz, T., Lutti, A., Phillips, C., et al. (2019). hmri—a toolbox  
743 for quantitative mri in neuroscience and clinical research. *NeuroImage*.

744 Thomas, A. G., Dennis, A., Rawlings, N. B., Stagg, C. J., Matthews, L., Morris,  
745 M., Kolind, S. H., Foxley, S., Jenkinson, M., Nichols, T. E., et al. (2016).  
746 Multi-modal characterization of rapid anterior hippocampal volume increase  
747 associated with aerobic exercise. *Neuroimage*, 131:162–170.

748 Todorow, M., DeSouza, J. F., Banwell, B. L., and Till, C. (2014).  
749 Interhemispheric cooperation in global-local visual processing in pediatric  
750 multiple sclerosis. *Journal of clinical and experimental neuropsychology*,  
751 36(2):111–126.

752 Turner, E. H., Matthews, A. M., Linardatos, E., Tell, R. A., and Rosenthal,  
753 R. (2008). Selective publication of antidepressant trials and its influence on  
754 apparent efficacy. *New England Journal of Medicine*, 358(3):252–260.

755 Vanes, L. D., Moutoussis, M., Ziegler, G., Goodyer, I. M., Fonagy, P., Jones,  
756 P. B., Bullmore, E. T., Consortium, N., and Dolan, R. J. (2020). White matter  
757 tract myelin maturation and its association with general psychopathology in  
758 adolescence and early adulthood. *Human brain mapping*, 41(3):827–839.

759 Wang, H., Liang, Y., Fan, W., Zhou, X., Huang, M., Shi, G., Yu, H., and Shen,  
760 G. (2019). Dti study on rehabilitation of the congenital deafness auditory  
761 pathway and speech center by cochlear implantation. *European Archives of  
762 Oto-Rhino-Laryngology*, 276(9):2411–2417.

763 Wedeen, V. J., Hagmann, P., Tseng, W.-Y. I., Reese, T. G., and Weisskoff, R. M.  
764 (2005). Mapping complex tissue architecture with diffusion spectrum magnetic  
765 resonance imaging. *Magnetic resonance in medicine*, 54(6):1377–1386.

766 Weiskopf, N., Callaghan, M. F., Josephs, O., Lutti, A., and Mohammadi,  
767 S. (2014). Estimating the apparent transverse relaxation time ( $r2^*$ ) from  
768 images with different contrasts (estatics) reduces motion artifacts. *Frontiers*  
769 *in neuroscience*, 8:278.

770 Weiskopf, N., Suckling, J., Williams, G., Correia, M. M., Inkster, B., Tait, R.,  
771 Ooi, C., Bullmore, E. T., and Lutti, A. (2013). Quantitative multi-parameter  
772 mapping of  $r1$ ,  $pd^*$ ,  $mt$ , and  $r2^*$  at 3t: a multi-center validation. *Frontiers in*  
773 *neuroscience*, 7:95.

774 Winkler, A. M., Ridgway, G. R., Webster, M. A., Smith, S. M., and Nichols,  
775 T. E. (2014). Permutation inference for the general linear model. *Neuroimage*,  
776 92:381–397.

777 Winkler, A. M., Webster, M. A., Brooks, J. C., Tracey, I., Smith, S. M., and  
778 Nichols, T. E. (2016). Non-parametric combination and related permutation  
779 tests for neuroimaging. *Human brain mapping*, 37(4):1486–1511.

780 Winston, G. P., Vos, S. B., Caldairou, B., Hong, S.-J., Czech, M., Wood, T. C.,  
781 Wastling, S. J., Barker, G. J., Bernhardt, B. C., Bernasconi, N., et al. (2020).  
782 Microstructural imaging in temporal lobe epilepsy: Diffusion imaging changes  
783 relate to reduced neurite density. *NeuroImage: Clinical*, page 102231.

784 Zatorre, R. J., Fields, R. D., and Johansen-Berg, H. (2012). Plasticity in gray  
785 and white: neuroimaging changes in brain structure during learning. *Nature  
786 neuroscience*, 15(4):528.